

FusionMamba: Dynamic Feature Enhancement for Multimodal Image Fusion with Mamba

Xinyu Xie
Great Bay University
Dongguan, China
18974784597@163.com

Yawen Cui
The Hong Kong Polytechnic University
Hong Kong, China
yawen.cui@polyu.edu.hk

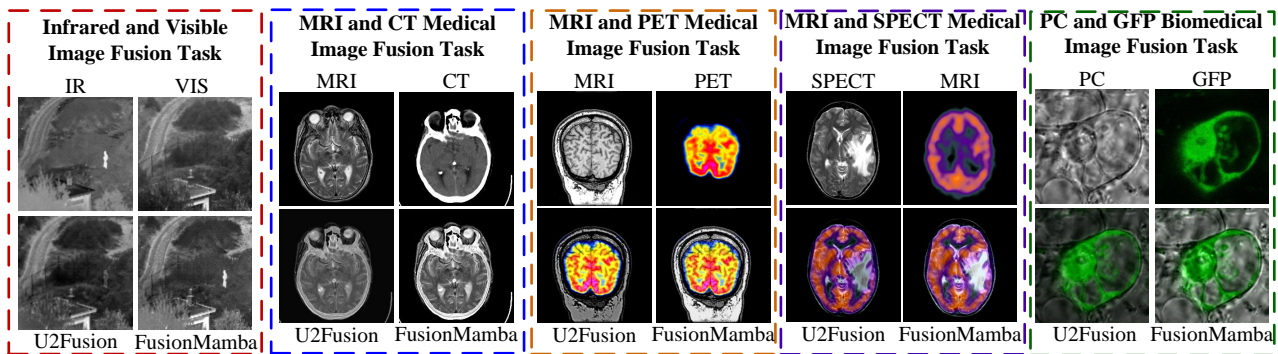
Chio-In IEONG
Guangdong Institute of Intelligence Science and Technology
Zhuhai, China
yangchaoran@gdiist.cn

Tao Tan
Macao Polytechnic University
Macao, China
taotansj@gmail.com

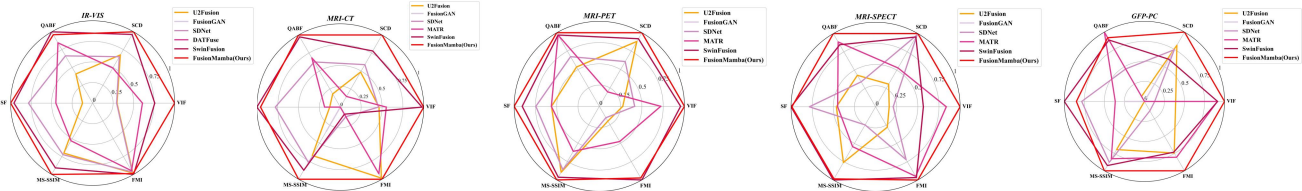
Xiaozhi Zhang
South China University
Hengyang, China
zxz_usc@163.com

Xubin Zheng
Great Bay University
Dongguan, China
xbzheng@gbu.edu.cn

Zitong Yu*
Great Bay University
Dongguan, China
yuzitong@gbu.edu.cn



(a) Visualizations of different multimodal image fusion tasks.



(b) Quantitative results

Figure 1. Illustration of qualitative and quantitative results of multi-modal image fusion. (a) Qualitative visualization between classical U2Fusion [30] and our FusionMamba is shown in the second row while the sub-figures on the first row are source image pairs. (b) Quantitative results imply the efficacy of FusionMamba over other methods on various datasets and metrics.

Abstract

Multi-modal image fusion aims to combine information from different modes to create a single image with comprehensive information and detailed textures. However, fusion models based on convolutional neural networks encounter limitations in capturing global image features due to their focus on local convolution operations. Transformer-based models,

while excelling in global feature modeling, confront computational challenges stemming from their quadratic complexity. Recently, the Selective Structured State Space Model has exhibited significant potential for long-range dependency modeling with linear complexity, offering a promising avenue to address the aforementioned dilemma. In this paper, we propose FusionMamba, a novel dynamic feature enhancement method for multimodal image fusion with Mamba. Specifically, we devise an improved efficient Mamba model for image fusion, integrating efficient visual state

*Corresponding author

space model with dynamic convolution and channel attention. This refined model not only upholds the performance of Mamba and global modeling capability but also diminishes channel redundancy while enhancing local enhancement capability. Additionally, we devise a dynamic feature fusion module (DFFM) comprising two dynamic feature enhancement modules (DFEM) and a cross modality fusion mamba module (CMFM). The former serves for dynamic texture enhancement and dynamic difference perception, whereas the latter enhances correlation features between modes and suppresses redundant intermodal information. FusionMamba has yielded state-of-the-art (SOTA) performance across various multimodal medical image fusion tasks (CT-MRI, PET-MRI, SPECT-MRI), infrared and visible image fusion task (IR-VIS) and multimodal biomedical image fusion dataset (GFP-PC), which is proved that our model has generalization ability. The code for FusionMamba is available at <https://github.com/millieXie/FusionMamba>.

CCS Concepts: • **Computing methodologies** → **Image fusion**.

Keywords: Multimodal, Image fusion, Feature enhancement, Mamba

1 Introduction

Different sensors capture unique data perspectives. Infrared sensors excel in thermal radiation capture, visible sensors in detailed texture data [36]. Medical imaging’s MRI and CT provide structural insights [39], while PET offers functional data [?]. Due to hardware limits, one sensor can’t capture the full image complexity [13]. Image fusion integrates source images to create informative ones. Infrared-Visible and Medical Image Fusion are crucial sub-categories [23], aiding diagnosis and enhancing images [36]. Fusion addresses sensitivity and noise issues, supporting practical applications [32–34].

In recent years, there has been a significant increase in the use of deep learning for multimodal image fusion, primarily employing CNNs [10, 30, 31, 37] and Transformer architectures [15, 24, 25, 27, 29] for feature extraction and reconstruction. However, these models face limitations. However, both types of models have inherent limitations. Specifically, the utilization of static convolutional layers in these fusion methods results in uniform traversal of the entire image, limiting their ability to capture global contextual information due to constrained receptive fields [15]. Moreover, the indiscriminate processing of each pixel by static convolutional layers overlooks nuanced spatial differences across various positions. Given the exigency of image fusion tasks necessitating diverse input data processing, current convolution-based techniques struggle to extract features effectively from different modalities, leading to diminished fusion performance. Transformer-based models excel in global modeling but suffer from quadratic complexity concerning image size due

to their self-attention mechanism [26], imposing substantial computational overhead. Additionally, Transformers exhibit lower precision in capturing local features compared to CNNs. Although certain fusion models [15, 27, 29, 38] adopt a hybrid approach by amalgamating convolutional and Transformer layers to leverage their respective strengths and mitigate weaknesses, computational overhead remains a significant concern.

Image fusion is an essential image enhancement technique [15]. Methodologies often employ three main feature fusion strategies. Firstly, some methods use element-wise operations like addition, multiplication, or concatenation [11, 37] to merge features from different modalities. However, these approaches overlook inter-modal relationships, leading to compromised fusion performance. Secondly, there are approaches that focus on deeper feature extraction [27, 29], but they still lack effective inter-modal interaction and texture detail emphasis. Lastly, specific techniques utilize cross-modal fusion [15], including convolution-based and Transformer-based methods, which partially address feature interaction but have their limitations. Overall, contemporary fusion methodologies struggle to optimally utilize modal features and highlight crucial information, indicating a need for improved modal connections and emphasis on key image details.

The advancement of Mamba [3] represents a promising avenue for achieving a balance between global receptive fields and computational efficiency. By formalizing the discretized state-space equations of Mamba into recursive form and incorporating specially designed structured reparameterization [6], it becomes capable of simulating very long-range dependencies. Moreover, the implementation of a parallel scanning algorithm [22] enables Mamba to process each token in a parallel manner, thereby facilitating efficient training on modern hardware like GPUs [18]. These encouraging characteristics inspire us to further explore Mamba’s potential for efficient long-range modeling within image fusion networks.

In response to the above issues, our study designs a new Dynamic Feature Enhancement Model with Mamba for multimodal image fusion, aimed at better exploring intra-modal and inter-modal features while dynamically enhancing the detail texture information of source images and the specificity information of each modality. Specifically, for the feature extraction and reconstruction part of the network, we design a Mamba model suitable for fusion tasks by integrating the Visual State Space Model with dynamic convolution and channel attention, not only maintaining Mamba’s performance and global modeling capabilities but also reducing channel redundancy and enhancing local feature extraction capabilities.

For the feature fusion part, we design a Dynamic Feature Fusion Module comprising a Dynamic Feature Enhancement Module and a Cross Modality Fusion Mamba Module. Unlike

previous feature fusion methods, this fusion module dynamically enhances the detail texture information and differential information in source images and facilitates better information interaction between modalities. The Dynamic Feature Enhancement Module (DFEM), composed of dynamic differential convolution and dynamic difference-sensing attention, is used for adaptive feature enhancement. The DFEM module dynamically enhances critical information by establishing connections between input features from different modalities. We design a Cross Modality Fusion Mamba Module to effectively mine correlation information between modalities. Our network architecture adopts a Unet [21] multi-layer structure, realizing an efficient and universal image fusion framework. Experimental results demonstrate that our proposed method outperforms state-of-the-art (SOTA) image fusion methods across various evaluation metrics on multiple multimodal baseline datasets, including IR-VIS fusion, CT-MRI fusion, PET-MRI fusion, SPECT-MRI fusion, and GFP-PC fusion.

In summary, our contributions encompass:

- We design a novel dynamic feature-enhanced Mamba image fusion model, this is the first improved state-space model for image fusion, offering a simple yet effective alternative to methods based on CNNs and Transformers.
- We propose the Dynamic Visual State Space (DVSS) block, which enhances the efficiency of the standard Mamba model by dynamically enhancing local features and reducing channel redundancy. This enhancement strengthens its modeling and feature extraction capabilities.
- The feature fusion module extracts key information from source images and explores relationships between different modalities. It includes a dynamic feature enhancement module for enhancing fine detail texture features and perceiving differential features, along with a cross-modal cross-Mamba fusion module for exploring inter-modal correlations effectively.
- We develop an efficient and versatile image fusion framework, achieving leading performance in various image fusion tasks, including infrared and visible light fusion, multi-modal medical image fusion, and biomedical image fusion.

2 Related Work

2.1 Deep Multimodal Image Fusion

Image fusion, as a critical image enhancement technology, has garnered significant attention in recent years [15]. In the era of deep learning, the primary image fusion methodologies can be categorized into four groups: Convolutional Neural Network (CNN) models [30, 31, 37], Generative Adversarial Network (GAN) models [16, 17], Autoencoder (AE) based models [10–12, 20], and models based on Transformer

architectures [15, 24, 27, 29, 38]. These methods often employ straightforward fusion rules like element addition, averaging, or multiplication [37]. While these convolutional methods can achieve satisfactory fusion results, they are limited in their ability to extract global features due to inherent convolution constraints [27]. Ma et al. [17] introduced an end-to-end GAN model named FusionGAN, where the source image is fed into the generation network, and the fusion result is generated by the discriminator network. Subsequently, they proposed a dual discriminator conditional generative adversarial network (DDcGAN) [16], which employs two discriminators to discern structural differences between the fused image and the two source images. While GANs demonstrate strong performance, their training process can be unstable, leading to potential texture distortion and difficulties in achieving stable fusion results due to the need to balance multi-source images using dual discriminators. Models based on autoencoders (AE) require a fusion rule to integrate features extracted from the encoder and generate the fusion result from the decoder. For example, RFN-Nest [12] introduced a two-stage learning strategy and a customizable fusion approach. Furthermore, researchers have explored Transformer-based methods, with IFT [27] and CDDFuse [38] effectively merging CNNs with Transformer architectures. SwinFusion [15] leverages SwinTransformer’s unique sliding window attention mechanism to address limitations in the convolutional fusion approach.

2.2 Mamba

State Space Models (SSMs) [4] have become a competitive backbone in deep learning, originating from classic control theory and offering linear scalability with sequence length for long-range dependency modeling. Structured State Space Sequence Models (S4) and Mamba [14], both rely on a classical continuous system that maps a 1D input function or sequence, denoted as $x(t) \in \mathbb{R}^L$, through intermediate implicit states $h(t) \in \mathbb{R}^L$ to an output $y(t) \in \mathbb{R}^L$. SSMs can be represented as the following linear Ordinary Differential Equation (ODE):

$$\begin{aligned} h'(t) &= \mathbf{A}h(t) + \mathbf{B}x(t), \\ y(t) &= \mathbf{C}h(t) + \mathbf{D}x(t) \end{aligned} \quad (1)$$

where $\mathbf{A} \in \mathbb{R}^{N \times N}$ represents the state matrix, while $\mathbf{B} \in \mathbb{R}^{N \times 1}$, $\mathbf{C} \in \mathbb{R}^{N \times 1}$, and $\mathbf{D} \in \mathbb{R}^N$ denote the projection parameters. After that, the discretization process is typically adopted into practical deep learning algorithms. Specifically, denote Δ as the timescale parameter to transform the continuous parameters \mathbf{A} , \mathbf{B} to discrete parameters $\bar{\mathbf{A}}$, $\bar{\mathbf{B}}$. The commonly used method for discretization is the zero-order hold (ZOH) rule, which is defined as follows:

$$\begin{aligned} \bar{\mathbf{A}} &= \exp(\Delta\mathbf{A}), \\ \bar{\mathbf{B}} &= (\Delta\mathbf{A})^{-1} (\exp(\Delta\mathbf{A}) - \mathbf{I}) \cdot \Delta\mathbf{B} \end{aligned} \quad (2)$$

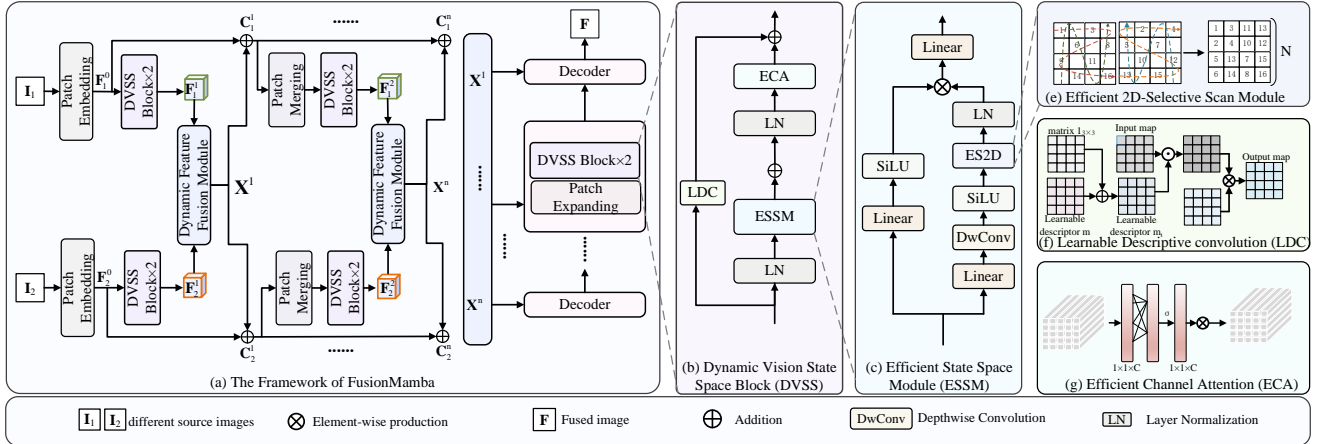


Figure 2. Overview of the framework. FusionMamba network receives two images of different modes as inputs. These images undergo multi-layer feature extraction and dynamic feature enhancement fusion through the fusion module, resulting in fusion features that include difference and texture enhancement. Finally, the module reconstructs the fusion result.

After the discretization, the discretized version of Eq. (1) with step size Δ can be rewritten in the following RNN form:

$$\begin{aligned} h_k &= \bar{\mathbf{A}}h_{k-1} + \bar{\mathbf{B}}x_k, \\ y_k &= \mathbf{C}h_k + \mathbf{D}x_k \end{aligned} \quad (3)$$

Furthermore, the Eq. (3) can also be mathematically equivalently transformed into the following CNN form:

$$\begin{aligned} \bar{\mathbf{K}} &\triangleq (\bar{\mathbf{C}}\bar{\mathbf{B}}, \bar{\mathbf{C}}\bar{\mathbf{A}}\bar{\mathbf{B}}, \dots, \bar{\mathbf{C}}\bar{\mathbf{A}}^{L-1}\bar{\mathbf{B}}), \\ \mathbf{y} &= \mathbf{x} \circledast \bar{\mathbf{K}} \end{aligned} \quad (4)$$

where \circledast denotes convolution operation, $\bar{\mathbf{K}} \in \mathbb{R}^L$ is a structured convolution kernel and L denotes the length of the input sequence \mathbf{x} .

Mamba has significantly advanced natural language tasks, surpassing traditional Transformers, with its data-dependent mechanisms, efficient hardware, and superior language processing. Expanding beyond language tasks, Mamba has also been applied successfully to vision tasks like image classification, video understanding, and biomedical image segmentation. This success has spurred a wave of research focusing on adapting Mamba-based models for specialized vision applications, including medical image segmentation with adaptations like Vm-unet [22]. Additionally, Mamba has been integrated into graph representation tasks, enhancing graph embeddings and processing capabilities through models. Mamba’s versatility and efficiency make it a compelling choice for a wide range of applications, from language processing to computer vision representation tasks [6, 18].

3 Methodology

3.1 Motivation

The motivation of this paper lies in addressing the common problems and challenges in the field of multimodal image fusion. In recent years, with the recognition of the powerful

capabilities of deep learning methods in image feature extraction, many fusion algorithms have emerged. However, the current mainstream convolutional neural networks (CNNs) [30, 31, 37] and Transformers models [15, 27, 29] have inherent limitations in image fusion, prompting us to delve into and design a new Dynamic Feature Enhancement Model to tackle these challenges and issues.

On the one hand, current fusion methods mainly use static convolutional layers for feature extraction and reconstruction, which have limitations in capturing nuanced spatial differences and global contextual information [5]. On the other hand, Transformer models excel in global modeling, but their quadratic complexity in image size due to the self-attention mechanism restricts their computational efficiency [22]. Additionally, they are less accurate in capturing local features compared to CNNs. Moreover, existing fusion methods also fall short in feature fusion, unable to effectively extract features from different modalities, leading to a decline in fusion performance.

Therefore, our motivation is to design a new Dynamic Feature Enhancement Model that combines the advantages of the Mamba model in global receptive fields and computational efficiency, along with dynamic feature enhancement and cross-modal fusion strategies. The goal is to better explore internal features and inter-modal relationships in multimodal image fusion, improve fusion performance, and overcome the limitations of current methods.

3.2 Overview

Our FusionMamba comprises three key components in the general fusion process: feature extraction, feature fusion, and feature reconstruction. The network architecture is based on the Unet framework to extract deeper features effectively. As illustrated in Fig. 2(a), both feature extraction and reconstruction phases utilize the designed Dynamic Vision State Space

(DVSS) modules. The feature fusion phase employs the Dynamic Feature Fusion module (DFFM, in Fig. 3). Each layer of the dynamic enhancement fusion module contains two Dynamic Feature Enhancement Modules (DFEM) and a Cross Modality Fusion Mamba module (CMFM). Therefore, in this section, we focus on introducing the designed dynamic vision state space module, dynamic feature enhancement module, and cross modality fusion Mamba module.

3.3 Dynamic Vision State Space Module

We propose the Dynamic Vision State Space (DVSS) module as a modification of the SSM block for image fusion processing. In Fig. 2(b), starting with the input deep feature, we initially apply LayerNorm (LN) followed by the Efficient State Space Module (ESSM) [18] to capture spatial long-term dependencies.

Since SSMs process flattened feature maps as 1D token sequences, the chosen flattening strategy significantly impacts the number of neighboring pixels in the sequence. For example, when using the four-direction unfolding strategy, only four nearest neighbors are accessible to the anchor pixel. Specially, efficient 2D scan (ES2D, in Fig. 2(e)) [18] efficiently downscales 2D-Selective-Scan (SS2D) using skipping sampling and combines processed patches for global feature extraction. Consequently, some spatially close pixels in the 2D feature map become distant from each other in the 1D token sequence, potentially resulting in local pixel forgetting. To tackle this issue, we introduce an additional dynamic local convolution after ES2D [18] to restore neighborhood similarity. The Learnable Descriptive Convolution (LDC, in Fig. 2(f)) effectively learns intricate textural features, making it highly suitable in here. we employ LayerNorm for normalization and then utilize Learnable Descriptive Convolution (LDC) [7] to compensate for local features.

Moreover, SSMs often introduce a larger number of hidden states to remember long-range dependencies, leading to significant channel redundancy when visualizing the activation results for different channels [14]. To enhance the expressive power of different channels, we integrate Efficient Channel Attention (ECA, in Fig. 2(g)) [28] into DVSS. This allows SSMs to concentrate on learning diverse channel representations, with subsequent channel attention selecting critical channels to prevent redundancy. DVSS is formulated as:

$$\mathbf{F}_D^{n+1} = \text{ECA}(\text{LN}(\text{ESSM}(\text{LN}(\mathbf{F}_D^n)))) + \text{LDC}(\mathbf{F}_D^n) \quad (5)$$

where \mathbf{F}_D^n represent the feature map of the n -layer and \mathbf{F}_D^{n+1} is the feature of the input at the next level. $\text{ESSM}(\cdot)$, $\text{LDC}(\cdot)$ and $\text{ECA}(\cdot)$ denotes the ESSM, LDC and ECA operations as shown in Fig. 2(c), Fig. 2(f) and Fig. (g), respectively.

3.4 Dynamic Feature Enhancement Module

The Dynamic Feature Enhancement Module (DFEM₁) for example) as shown in Fig. 4, aiming to improve texture detail

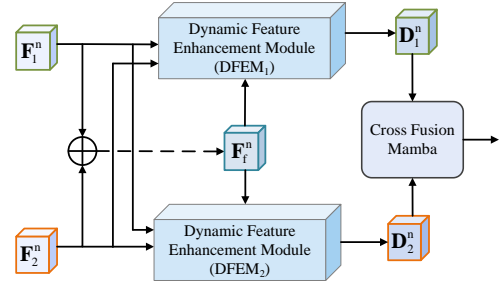


Figure 3. Dynamic Feature Fusion Module (DFFM).

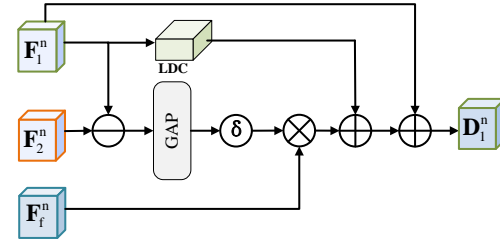


Figure 4. Dynamic Feature Enhancement Module (DFEM).

features adaptively through a dynamic feature enhancement mechanism and dynamically perceive differences between different modes. Specifically, DFEM₁ takes two different modes of features (\mathbf{F}_1^n , \mathbf{F}_2^n) as inputs and performs coarse-grained fusion feature (\mathbf{F}_f^n) in the module. By subtracting elements from different modal features to obtain difference features, the mapping of these difference features is enhanced. Subsequently, these difference features are merged with the original features, enriching the difference features with additional modal supplemental information. This process effectively extracts and amplifies inherent complementary features and texture details in images, thereby enhancing overall fusion performance.

Within the module, the Learnable Descriptive Convolution (LDC) [7] module enhances texture processing on input feature maps using learnable mask parameters and convolution operations. By adjusting the convolution kernel's weights, it emphasizes texture information, enhancing the model's texture feature perception. Conversely, the Dynamic Difference Perception Attention calculates difference weights between input feature maps and applies them to both fused and original features, amplifying feature differences. This method helps the model effectively capture subtle differences among input features, leading to improved resolution and perception across different features and contributing to the model's enhanced fusion performance. Finally, DFEM₁ combines the texture enhancement feature, difference enhancement feature, and low-frequency feature (\mathbf{F}_1^n) with background information, outputting \mathbf{D}_1^n .

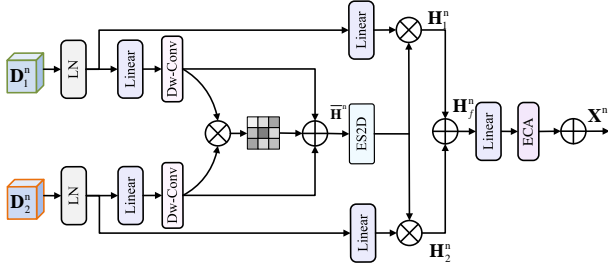


Figure 5. Cross Modality Fusion Mamba Module (CMFM).

3.5 Cross Modality Fusion Mamba Module

The features output by the dynamic feature enhancement module (DFEM, in Fig. 4) are further fed into the Cross Modality Fusion Mamba (CMFM, in Fig. 5) module for fine-grained fusion and exploration of information correlation between different modalities. The enhanced features (D_1^n , D_2^n) of the different modes are first mixed to generate the mixed features \overline{H}^n :

$$\overline{H}^n = \text{Dwc}(\text{Linear}(D_1^n)) \otimes \text{Dwc}(\text{Linear}(D_2^n)) \oplus D_1^n \oplus D_2^n \quad (6)$$

where $\text{Dwc}(\cdot)$ is the Depthwise convolution operation. \otimes and \oplus are the Element-wise multiplication and addition operation.

These hybrid enhanced features are then input into the Efficient Spatial Scanning 2D (ES2D) [?] layer to capture the spatial long-term dependency.

$$\begin{aligned} H_1^n &= \text{LN}\left(\text{ES2D}\left(\text{SiLU}\left(\overline{H}^n\right)\right)\right) \otimes \text{SiLU}\left(\text{Linear}\left(D_1^n\right)\right), \\ H_2^n &= \text{LN}\left(\text{ES2D}\left(\text{SiLU}\left(\overline{H}^n\right)\right)\right) \otimes \text{SiLU}\left(\text{Linear}\left(D_2^n\right)\right), \quad (7) \\ H_f^n &= H_1^n \oplus H_2^n \end{aligned}$$

The output features pass through a Channel Attention module (ECA) to reduce channel redundancy, resulting in the final fused feature map (X^n):

$$X^n = \text{ECA}\left(\text{LN}\left(H_f^n\right)\right) \oplus D_1^n \oplus D_2^n \quad (8)$$

3.6 Loss Function

To ensure the extraction of meaningful information during training, we introduce three types of loss functions: the intensity loss \mathcal{L}_{int} , the texture loss $\mathcal{L}_{\text{text}}$, and the structure loss $\mathcal{L}_{\text{ssim}}$. The total loss $\mathcal{L}_{\text{total}}$ can be shown as follow:

$$\mathcal{L}_{\text{total}} = \alpha_1 \mathcal{L}_{\text{int}} + \alpha_2 \mathcal{L}_{\text{text}} + \alpha_3 \mathcal{L}_{\text{ssim}} \quad (9)$$

where α_1 , α_2 , and α_3 are the weights to control the trade-off between \mathcal{L}_{int} , $\mathcal{L}_{\text{text}}$ and $\mathcal{L}_{\text{ssim}}$.

Integrating more texture details is essential to improve visual quality. We use gradient loss to ensure that more fine-grained details are preserved, which is defined as

$$\mathcal{L}_{\text{text}} = \frac{1}{HW} \|\nabla I_f - \max(\nabla |I_1|, \nabla |I_2|)\|_1 \quad (10)$$

Generally, there is significant intensity information and contrast information in source images. We employ intensity loss to ensure that appropriate intensity information is retained. It can be defined as

$$\mathcal{L}_{\text{int}} = \frac{1}{HW} \|I_f - \max(I_1, I_2)\|_2 \quad (11)$$

SSIM [2] can measure the degree of distortion and the degree of similarity between two images. We use SSIM loss to guarantee structure similarity between the fused image and source images. It can be defined as

$$\mathcal{L}_{\text{ssim}} = \frac{1}{2}(1 - \text{SSIM}(I_1, I_f)) + \frac{1}{2}(1 - \text{SSIM}(I_2, I_f)) \quad (12)$$

4 Experiment

4.1 Setup

4.1.1 Datasets. we choose the KAIST [8] dataset to train our FusionMamba. In this dataset, 70000 pairs of infrared and visible images are chosen for training. These images are also converted to gray scale and resized to 256×256 . We use Harvard Medical Dataset ¹ as the training and test dataset independently. There are 166 CT-MRI image pairs, 329 PET-MRI image pairs and 539 SPECT-MRI image pairs. The size of images is 256×256 . We augment image pairs to 30000 via image rotation, which can improve the model and help to combat potential overfitting. 21 pairs of test images are randomly chosen to evaluate the model. The GFP database1 released by John Innes Centre [9] is employed in our experiments. The database contains 148 pairs of preregistered GFP and PC images of Arabidopsis thaliana cells with the same size of 358×358 pixels. We also augment image pairs to 30000 via image rotation. 20 pairs of test images are randomly chosen to evaluate the model.

4.1.2 Implementation Details and Metrics. The batch size is 4 and Adam optimizer with a learning rate 0.0001 is used. α_1 , α_2 , and α_3 are set as 1,1,10. The experiments are conducted using Nvidia GeForce RTX 3090 GPU and 3.60 GHz Intel Core i9-9900K CPU with Pytorch.

Fusion performance is evaluated using six key metrics [2, 19]: Structural Fidelity (SF), Structure Content Difference (SCD), Multiscale Structural Similarity Index Measure (MS-SSIM), Gradient-Based Metric ($Q^{AB/F}$), Feature Mutual Information (FMI), and Visual Information Fidelity (VIF) [1]. These metrics evaluate fusion performance from multiple perspectives, including structural preservation, content difference, feature information, and visual fidelity in the fused image compared to source images. SF measures structural fidelity, SCD quantifies content difference, MS-SSIM evaluates structural similarity across scales, $Q^{AB/F}$ assesses edge information retention, FMI measures feature information preservation, and VIF calculates visual fidelity comprehensively.

¹<http://www.med.harvard.edu/AANLIB/home.html>

Table 1. Comparison results in the CT-MRI Task. Best results are marked in **bold**.

| Method | VIF \uparrow | SCD \uparrow | $Q^{AB/F}$ \uparrow | SF \uparrow | MS-SSIM \uparrow | FMI \uparrow |
|---------------------------|----------------|----------------|-----------------------|----------------|--------------------|----------------|
| CSMCA [13] | 0.4745 | 1.1372 | 0.5986 | 30.2602 | 0.9444 | 0.8800 |
| U2F [30] | 0.4246 | 0.8399 | 0.2865 | 14.8600 | 0.8355 | 0.8619 |
| FGAN [17] | 0.2597 | 0.1318 | 0.2068 | 12.1149 | 0.7234 | 0.8308 |
| SDNet [35] | 0.4224 | 0.9895 | 0.4797 | 28.9928 | 0.8672 | 0.8350 |
| MATR [24] | 0.4556 | 0.3468 | 0.5044 | 16.1920 | 0.6095 | 0.8600 |
| SwinF [15] | 0.6075 | 1.2659 | 0.6312 | 32.8764 | 0.9042 | 0.8339 |
| IFT [27] | 0.5016 | 1.1188 | 0.4571 | 21.4474 | 0.8928 | 0.8687 |
| FusionMamba (Ours) | 0.5750 | 1.58884 | 0.6429 | 32.8227 | 0.9462 | 0.8624 |

Table 2. Comparison results in the PET-MRI Task. Best results are marked in **bold**.

| Method | VIF \uparrow | SCD \uparrow | $Q^{AB/F}$ \uparrow | SF \uparrow | MS-SSIM \uparrow | FMI \uparrow |
|---------------------------|----------------|----------------|-----------------------|----------------|--------------------|----------------|
| CSMCA [13] | 0.5515 | 0.7892 | 0.6505 | 29.4565 | 0.9156 | 0.8401 |
| U2F [30] | 0.4618 | 1.2809 | 0.5153 | 26.3977 | 0.9074 | 0.8232 |
| FGAN [17] | 0.3742 | 0.4620 | 0.2563 | 16.9172 | 0.6603 | 0.8127 |
| SDNet [35] | 0.5061 | 1.0270 | 0.5831 | 29.5060 | 0.8971 | 0.8208 |
| MATR [24] | 0.6033 | 0.6442 | 0.7254 | 26.4280 | 0.8290 | 0.8377 |
| SwinF [15] | 0.6775 | 1.3148 | 0.7254 | 32.2117 | 0.9261 | 0.8650 |
| IFT [27] | 0.6149 | 1.4068 | 0.5501 | 21.5242 | 0.9129 | 0.8431 |
| FusionMamba (Ours) | 0.6920 | 1.3906 | 0.7406 | 33.8087 | 0.9362 | 0.8616 |

These metrics together offer a comprehensive evaluation of fusion performance across different criteria.

4.1.3 Comparison Approaches. We perform extensive comparison experiments with state-of-the-art methods to demonstrate the validity of FusionMamba. These comparison methods include CSMCA [13], U2Fusion [30], FusionGAN [17], SDNet [35], MATR [24], IFT [27] and SwinFusion [15]. CSMCA [13] is the traditional fusion method. SDNet [35], FusionGAN, and U2Fusion [30] are CNN-based fusion methods. MATR [24], IFT and SwinFusion [15] are Transformer-based structures. We use the public codes with corresponding parameter settings.

4.2 Multimodal Medical Image Fusion

We present three typical medical image fusion tasks: CT-MRI image fusion, PET-MRI image fusion, and SPECT-MRI image fusion tasks. The qualitative and quantitative results are shown in Fig. 6 and Table I, respectively.

For the qualitative analysis, the first row in Fig. 6 displays the CT-MRI fusion task, including CT images, MRI images, and the fusion results of CSMCA [13], U2Fusion [30], FusionGAN [17], SDNet [35], MATR [24], SwinFusion [15], IFT [27], and the proposed FusionMamba. We zoomed in on the area in the red box, demonstrating that our fusion images can simultaneously retain the dense information of CT and the texture details of MRI. In Fig. 6, FusionGAN and U2Fusion [30] exhibit unsatisfactory brightness and clarity, with some gray matter blurring the texture details. Particularly, FusionGAN shows artifacts and redundant information. MATR [24] preserves structural details but weakens dense structures. SDNet [35] and CSMCA [13] retain dense structures but lose some edge details. SwinFusion [15] achieves satisfactory fusion but with excessively sharp edges. In contrast, our FusionMamba retains more texture details while

Table 3. Comparison results in the SPECT-MRI Task. Best results are marked in **bold**.

| Method | VIF \uparrow | SCD \uparrow | $Q^{AB/F}$ \uparrow | SF \uparrow | MS-SSIM \uparrow | FMI \uparrow |
|---------------------------|----------------|----------------|-----------------------|----------------|--------------------|----------------|
| CSMCA [13] | 0.6051 | 0.1854 | 0.6301 | 13.708 | 0.9144 | 0.8827 |
| U2F [30] | 0.4525 | 0.5633 | 0.4789 | 12.7316 | 0.9209 | 0.8600 |
| FGAN [17] | 0.3879 | 0.2734 | 0.3059 | 10.0998 | 0.8065 | 0.8484 |
| SDNet [35] | 0.4715 | 1.1937 | 0.4430 | 14.5479 | 0.8437 | 0.8785 |
| MATR [24] | 0.7235 | 0.1706 | 0.6620 | 12.6463 | 0.8883 | 0.8880 |
| SwinF [15] | 0.6147 | 1.1665 | 0.6468 | 15.7775 | 0.9568 | 0.8887 |
| IFT [27] | 0.6024 | 1.1504 | 0.6127 | 12.7114 | 0.9196 | 0.8770 |
| FusionMamba (Ours) | 0.7891 | 1.2106 | 0.7080 | 15.7195 | 0.9545 | 0.8901 |

maintaining appropriate dense structures. Visually, they appear more natural with enhanced contrast.

The second row in Fig. 6 presents the PET-MRI fusion task. FusionGAN’s fusion images have lower contrast and missing texture details, while CSMCA [13] and IFT [27] preserve texture information well. However, the darker color indicates insufficient preservation of functional information. Additionally, IFT [27], U2Fusion [30], and SDNet [35] retain functional features but with less sharp texture details in salient regions. SwinFusion [15] shows color distortion due to over-sharpening. In contrast, our FusionMamba preserves clear edges and texture details, with a color distribution more similar to PET images, enhancing visual perception.

Moving to the third row, focusing on the SPECT-MRI fusion task, similar to PET-MRI fusion, our FusionMamba excels in capturing more details and retaining appropriate color information from SPECT images.

Table I displays the quantitative comparison results for six metrics in the CT-MRI fusion task. FusionMamba achieves optimal results (average values) in VIF, SCD, $Q^{AB/F}$, SF, MS-SSIM, and FMI, indicating higher structure similarity, enhanced contrast, and better visual effects. Similar trends are observed in Table II for the PET-MRI fusion task and Table III for the SPECT-MRI fusion task, where FusionMamba consistently outperforms other methods across various metrics, demonstrating superior fusion performance in retaining functional and morphological information.

Overall, FusionMamba achieves better fusion performance, including richer information retention and improved visual effects, across all evaluated tasks.

4.3 Infrared and Visible Image Fusion

Fig. 7 and Table 4 illustrate that RFN-Nest[12], DATFuse [25], SDNet [35], and U2Fusion [30] struggle to accurately represent scene information in visible images due to inadequate global information interaction and improper intensity control. On the other hand, while IFT [27] and SwinFusion [15] manage to preserve some texture details in visible images, they are still susceptible to contamination from thermal radiation, resulting in a reduction in the clarity of infrared image targets to varying extents.

It is important to note that our FusionMamba method excels in retaining both the scene information of visible images and the salient objects, achieved through effective

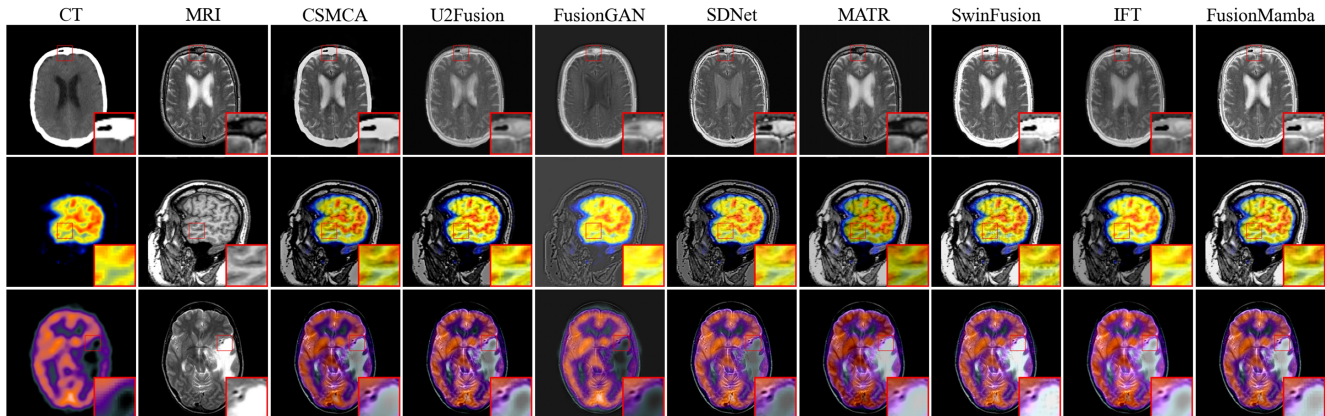


Figure 6. Qualitative results on fusion of multimodal medical images.

Table 4. Comparison results in the IR-VIS Task. Best results are marked in **bold**.

| Method | VIF \uparrow | SCD \uparrow | $Q^{AB/F}$ \uparrow | SF \uparrow | MS-SSIM \uparrow | FMI \uparrow |
|---------------------------|----------------|----------------|-----------------------|----------------|--------------------|----------------|
| RFN [12] | 0.612 | 1.6109 | 0.4229 | 11.3723 | 0.8544 | 0.8751 |
| U2F [30] | 0.4736 | 1.6390 | 0.3539 | 7.0651 | 0.8343 | 0.8836 |
| FGAN [17] | 0.3476 | 1.2372 | 0.2107 | 5.6672 | 0.5314 | 0.6701 |
| SDNet [35] | 0.4715 | 1.6237 | 0.4430 | 14.5479 | 0.8436 | 0.8785 |
| DATF [25] | 0.6052 | 1.5297 | 0.5071 | 10.7585 | 0.7595 | 0.8730 |
| SwinF [15] | 0.6687 | 1.8095 | 0.5611 | 16.5580 | 0.9236 | 0.8894 |
| IFT [27] | 0.6350 | 1.7817 | 0.4668 | 11.0382 | 0.8606 | 0.8853 |
| FusionMamba (Ours) | 0.7717 | 1.8314 | 0.5468 | 17.0171 | 0.9331 | 0.8858 |

global context awareness and dynamic feature enhancement. Specifically, our model dynamically focuses on significant areas in infrared images while preserving texture details in visible images.

4.4 Multimodal Biomedical Image Fusion

To demonstrate the generalization capability of FusionMamba, we conduct green fluorescent protein (GFP) and phase contrast (PC) image fusion. GFP images provide functional information related to protein distribution, while PC images contain rich details of cell structure including nucleus and mitochondria. GFP and PC fusion images can promote biological research such as gene expression and protein function analysis. In Figure 8 and Table 5, it can be found that FusionGAN [17], U2Fusion [30] and IFT [27] can well preserve color information, but there is a certain loss of texture details. U2Fusion [30] and MATR [24] can well retain texture details, but there is slight color distortion. It is worth noting that both SwinFusion [15] and FusionMamba can effectively preserve texture and color information, which proves the effectiveness of cross fusion strategies in image fusion.

4.5 Computational Cost Analysis

The complexity evaluation in Table 6 assesses the operational efficiency of various methods by measuring floating-point operations per second (FLOPs) and running time. Specifically, the first image in the dataset undergoes testing within an infrared and visible light fusion scenario to compute the FLOPs of each method. We compare the CNN-based U2Fusion [30],

Table 5. Comparison results in the GFP-PC Task. Best results are marked in **bold**.

| Method | VIF \uparrow | SCD \uparrow | $Q^{AB/F}$ \uparrow | SF \uparrow | MS-SSIM \uparrow | FMI \uparrow |
|---------------------------|----------------|----------------|-----------------------|----------------|--------------------|----------------|
| CSMCA [13] | 0.7609 | 1.4303 | 0.6475 | 11.1794 | 0.9453 | 0.8723 |
| U2F [30] | 0.6085 | 1.3442 | 0.3329 | 6.2236 | 0.8562 | 0.8616 |
| FGAN [17] | 0.4538 | 1.2913 | 0.3027 | 8.6908 | 0.6823 | 0.8358 |
| SDNet [35] | 0.5046 | 1.3040 | 0.4983 | 14.0584 | 0.9023 | 0.8405 |
| MATR [24] | 0.8147 | 0.8400 | 0.7205 | 9.8661 | 0.8893 | 0.8637 |
| SwinF [15] | 0.8159 | 1.2185 | 0.6727 | 16.2299 | 0.9138 | 0.8612 |
| IFT [27] | 0.5652 | 1.3588 | 0.4659 | 12.0810 | 0.8993 | 0.8368 |
| FusionMamba (Ours) | 0.8503 | 1.4623 | 0.6863 | 14.7204 | 0.9328 | 0.8705 |

Table 6. Computational cost analysis.

| Method | U2F [30] | IFCNN [37] | IFT [27] | SwinF [15] | FusionMamba (Ours) |
|--------------|----------|------------|----------|------------|--------------------|
| Run Time (s) | 0.20 | 0.19 | 0.36 | 0.23 | 0.13 |
| Flops (G) | 345.75 | 77.94 | 184.56 | 135.17 | 16.50 |

IFCNN [37] method with the Transformer-based IFT [27] and SwinFusion [15] method. The results reveal a notable advantage of the Mamba-based approach in terms of runtime, showcasing lower FLOPs and average uptime compared to CNN and Transformer methods. Importantly, our method demonstrates superior fusion performance when compared to mainstream image fusion algorithms.

5 Ablation Experiments

5.1 Structure Ablation

To analyze the network architecture better, we conduct 5 sets of ablation experiments, as shown in Table 7. To validate DVSS effectiveness, we perform two additional experiments: EVSS [18] and replacing DVSS with Transformer (Case 1 and Case 2). EVSS produces satisfactory results, but it's less effective than DVSS in design due to DVSS's stronger feature extraction capability. Replacing DVSS with the Transformer network leads to a decline in metrics. The proposed DFFM significantly enhances fusion effect, as seen in Case 3 where its absence causes a decrease in SF and $Q^{AB/F}$. Removing the DFEM module (Case 4) shows similar results to not having DFFM. The Mamba module for cross-modal fusion is vital for effective information integration, as networks without Mamba module integration (Case 5) show degraded VIF task

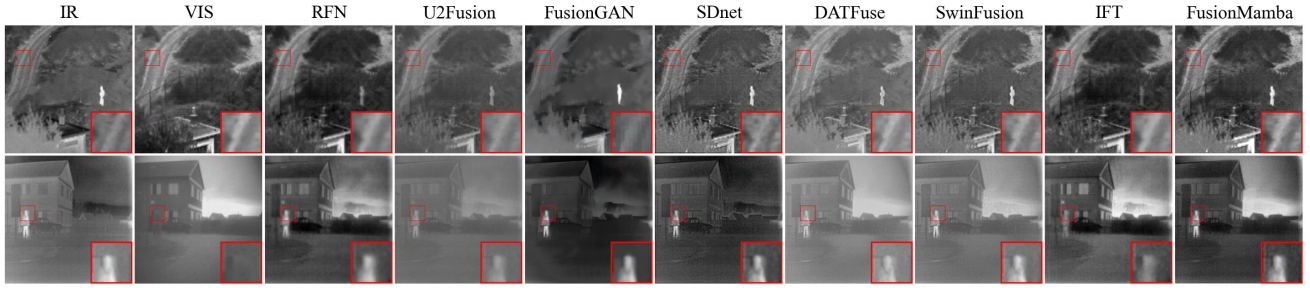


Figure 7. Qualitative results on fusion of three typical IR and VIS images.

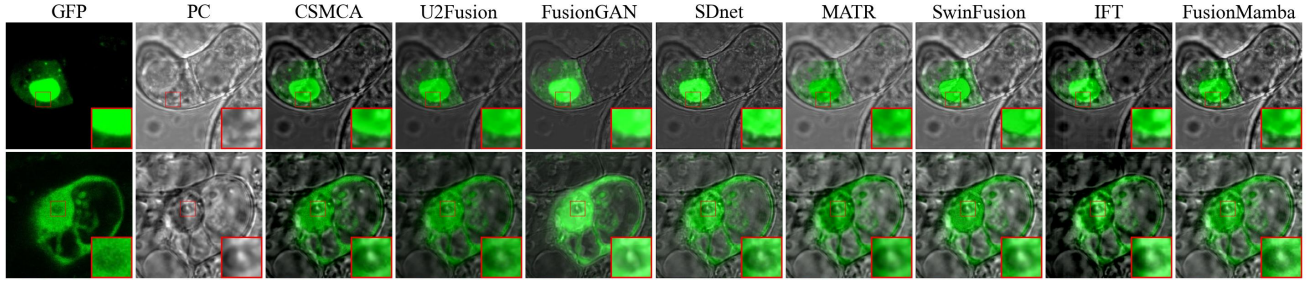


Figure 8. Qualitative results on fusion of three typical GFP and PC images.

Table 7. The ablation of network structure.

| Method | VIF \uparrow | SCD \uparrow | $Q^{AB/F}$ \uparrow | SF \uparrow | MS-SSIM \uparrow | FMI \uparrow |
|--------------------------------|----------------|----------------|-----------------------|---------------|--------------------|----------------|
| DVSS \rightarrow EVSS | 0.6809 | 1.7917 | 0.5086 | 16.8729 | 0.9006 | 0.8625 |
| DVSS \rightarrow Transformer | 0.6701 | 1.7329 | 0.5014 | 16.7061 | 0.8812 | 0.8334 |
| DFFM \rightarrow DVSS | 0.7334 | 1.7881 | 0.5220 | 16.9880 | 0.8990 | 0.8417 |
| w/o DFEM | 0.7459 | 1.7412 | 0.5129 | 16.6911 | 0.8774 | 0.8719 |
| w/o CMFM | 0.7016 | 1.7615 | 0.5231 | 16.7907 | 0.8895 | 0.8751 |
| FusionMamba | 0.7717 | 1.8314 | 0.5468 | 17.0171 | 0.9331 | 0.8858 |

Table 8. The ablation of Loss Function.

| Method | VIF \uparrow | SCD \uparrow | $Q^{AB/F}$ \uparrow | SF \uparrow | MS-SSIM \uparrow | FMI \uparrow |
|--------------------------|----------------|----------------|-----------------------|---------------|--------------------|----------------|
| w/o \mathcal{L}_{ssim} | 0.7702 | 1.6773 | 0.5501 | 15.7055 | 0.8260 | 0.8802 |
| w/o \mathcal{L}_{int} | 0.6673 | 1.8216 | 0.5448 | 15.6387 | 0.8994 | 0.8804 |
| w/o \mathcal{L}_{sxt} | 0.5235 | 1.8283 | 0.4604 | 15.0716 | 0.9158 | 0.8862 |
| FusionMamba | 0.7717 | 1.8314 | 0.5468 | 17.0171 | 0.9331 | 0.8858 |

visual performance. Absence of CMFM leads to a decrease in MS-SSIM of fused images, indicating the importance of cross-domain integration for perceiving key goals and structures in fusion tasks.

5.2 Loss Ablation

We conduct ablation experiments on each loss function to evaluate its impact, as depicted in Table 8. Initially, we introduce SSIM loss (\mathcal{L}_{ssim}) to constrain the fusion network, preserving structural information in the source image. Furthermore, SSIM loss helps control the brightness of fusion results to some extent. Networks lacking structural constraints struggle to maintain optimal structure and strength information, leading to a decrease in MS-SSIM scores. Texture loss (\mathcal{L}_{text}) contributes significantly to retaining edge information in the fusion result, thereby enhancing clarity. Without texture loss, we observe significant decreases in $Q^{AB/F}$ and SF metrics. Excluding intensity loss (\mathcal{L}_{int}) from the joint loss function diminishes the visual impact of the fused image. Our model consistently outperforms other versions across all metrics, highlighting the optimal performance of our proposed loss function.

6 Conclusion

In conclusion, our study addresses the challenges of multimodal image fusion by proposing FusionMamba, a novel dynamic feature enhancement method integrated with the Mamba framework. Our approach combines an improved efficient Mamba model with dynamic convolution and channel attention, enhancing both global modeling capabilities and local feature extraction. We also introduce a dynamic feature fusion module (DFFM) that includes two dynamic feature enhancement modules (DFEM) and a cross-modality fusion Mamba module (CMFM), effectively enhancing texture, perception of differences, and correlation between modalities while suppressing redundant information. Our FusionMamba method has demonstrated state-of-the-art (SOTA) performance in various multimodal image fusion tasks. These results validate the generalization ability of our proposed method. For future work, we aim to investigate the application of FusionMamba in real-time scenarios and deploying it on resource-constrained devices would be beneficial for practical implementation. Furthermore, extending our evaluation to more diverse datasets and benchmarking against emerging fusion methods would provide a comprehensive understanding of the capabilities of FusionMamba.

References

- [1] Hao Chen and Pramod K Varshney. 2007. A human perception inspired quality metric for image fusion based on regional information. *Information fusion* 8, 2 (2007), 193–207.
- [2] Nedeljko Cvejic, Artur Loza, David Bull, and Nishan Canagarajah. 2005. A similarity metric for assessment of image fusion algorithms. *International journal of signal processing* 2, 3 (2005), 178–182.
- [3] Albert Gu and Tri Dao. 2023. Mamba: Linear-time sequence modeling with selective state spaces. *arXiv preprint arXiv:2312.00752* (2023).
- [4] Albert Gu, Isys Johnson, Karan Goel, Khaled Saab, Tri Dao, Atri Rudra, and Christopher Ré. 2021. Combining recurrent, convolutional, and continuous-time models with linear state space layers. *Advances in neural information processing systems* 34 (2021), 572–585.
- [5] Yuanshen Guan, Ruikang Xu, Mingde Yao, Lizhi Wang, and Zhiwei Xiong. 2023. Mutual-guided dynamic network for image fusion. In *Proceedings of the 31st ACM International Conference on Multimedia*. 1779–1788.
- [6] Hang Guo, Jinmin Li, Tao Dai, Zhihao Ouyang, Xudong Ren, and Shu-Tao Xia. 2024. MambaIR: A Simple Baseline for Image Restoration with State-Space Model. *arXiv preprint arXiv:2402.15648* (2024).
- [7] Pei-Kai Huang, Hui-Yu Ni, Yanqin Ni, and Chiou-Ting Hsu. 2022. Learnable Descriptive Convolutional Network for Face Anti-Spoofing.. In *BMVC*. 239.
- [8] Soonmin Hwang, Jaesik Park, Namil Kim, Yukyung Choi, and In So Kweon. 2015. Multispectral pedestrian detection: Benchmark dataset and baseline. In *Proceedings of the IEEE conference on computer vision and pattern recognition*. 1037–1045.
- [9] Olga A Koroleva, Matthew L Tomlinson, David Leader, Peter Shaw, and John H Doonan. 2005. High-throughput protein localization in Arabidopsis using Agrobacterium-mediated transient expression of GFP-ORF fusions. *The Plant Journal* 41, 1 (2005), 162–174.
- [10] Hui Li and Xiao-Jun Wu. 2018. DenseFuse: A fusion approach to infrared and visible images. *IEEE Transactions on Image Processing* 28, 5 (2018), 2614–2623.
- [11] Hui Li, Xiao-Jun Wu, and Tariq Durrani. 2020. NestFuse: An infrared and visible image fusion architecture based on nest connection and spatial/channel attention models. *IEEE Transactions on Instrumentation and Measurement* 69, 12 (2020), 9645–9656.
- [12] Hui Li, Xiao-Jun Wu, and Josef Kittler. 2021. RFN-Nest: An end-to-end residual fusion network for infrared and visible images. *Information Fusion* 73 (2021), 72–86.
- [13] Yu Liu, Xun Chen, Rabab K Ward, and Z Jane Wang. 2019. Medical image fusion via convolutional sparsity based morphological component analysis. *IEEE Signal Processing Letters* 26, 3 (2019), 485–489.
- [14] Yue Liu, Yunjie Tian, Yuzhong Zhao, Hongtian Yu, Lingxi Xie, Yaowei Wang, Qixiang Ye, and Yunfan Liu. 2024. Vmamba: Visual state space model. *arXiv preprint arXiv:2401.10166* (2024).
- [15] Jiayi Ma, Linfeng Tang, Fan Fan, Jun Huang, Xiaoguang Mei, and Yong Ma. 2022. SwinFusion: Cross-domain long-range learning for general image fusion via swin transformer. *IEEE/CAA Journal of Automatica Sinica* 9, 7 (2022), 1200–1217.
- [16] Jiayi Ma, Han Xu, Junjun Jiang, Xiaoguang Mei, and Xiao-Ping Zhang. 2020. DDcGAN: A dual-discriminator conditional generative adversarial network for multi-resolution image fusion. *IEEE Transactions on Image Processing* 29 (2020), 4980–4995.
- [17] Jiayi Ma, Wei Yu, Pengwei Liang, Chang Li, and Junjun Jiang. 2019. FusionGAN: A generative adversarial network for infrared and visible image fusion. *Information fusion* 48 (2019), 11–26.
- [18] Xiaohuan Pei, Tao Huang, and Chang Xu. 2024. EfficientVMamba: Atrous Selective Scan for Light Weight Visual Mamba. *arXiv preprint arXiv:2403.09977* (2024).
- [19] Gemma Piella and Henk Heijmans. 2003. A new quality metric for image fusion. In *Proceedings 2003 international conference on image processing (Cat. No. 03CH37429)*, Vol. 3. IEEE, III–173.
- [20] K Ram Prabhakar, V Sai Srikar, and R Venkatesh Babu. 2017. Deepfuse: A deep unsupervised approach for exposure fusion with extreme exposure image pairs. In *Proceedings of the IEEE international conference on computer vision*. 4714–4722.
- [21] Olaf Ronneberger, Philipp Fischer, and Thomas Brox. 2015. U-net: Convolutional networks for biomedical image segmentation. In *Medical image computing and computer-assisted intervention—MICCAI 2015: 18th international conference, Munich, Germany, October 5–9, 2015, proceedings, part III 18*. Springer, 234–241.
- [22] Jiacheng Ruan and Suncheng Xiang. 2024. Vm-unet: Vision mamba unet for medical image segmentation. *arXiv preprint arXiv:2402.02491* (2024).
- [23] Linfeng Tang, Xinyu Xiang, Hao Zhang, Meiqi Gong, and Jiayi Ma. 2023. DIVFusion: Darkness-free infrared and visible image fusion. *Information Fusion* 91 (2023), 477–493.
- [24] Wei Tang, Fazhi He, Yu Liu, and Yansong Duan. 2022. MATR: Multimodal medical image fusion via multiscale adaptive transformer. *IEEE Transactions on Image Processing* 31 (2022), 5134–5149.
- [25] Wei Tang, Fazhi He, Yu Liu, Yansong Duan, and Tongzhen Si. 2023. DATFuse: Infrared and visible image fusion via dual attention transformer. *IEEE Transactions on Circuits and Systems for Video Technology* (2023).
- [26] Ashish Vaswani, Noam Shazeer, Niki Parmar, Jakob Uszkoreit, Llion Jones, Aidan N Gomez, Lukasz Kaiser, and Illia Polosukhin. 2017. Attention is all you need. *Advances in neural information processing systems* 30 (2017).
- [27] Vibashan Vs, Jeya Maria Jose Valanarasu, Poojan Oza, and Vishal M Patel. 2022. Image fusion transformer. In *2022 IEEE International conference on image processing (ICIP)*. IEEE, 3566–3570.
- [28] Qilong Wang, Banggu Wu, Pengfei Zhu, Peihua Li, Wangmeng Zuo, and Qinghua Hu. 2020. ECA-Net: Efficient channel attention for deep convolutional neural networks. In *Proceedings of the IEEE/CVF conference on computer vision and pattern recognition*. 11534–11542.
- [29] Xinyu Xie, Xiaozhi Zhang, Shengcheng Ye, Dongping Xiong, Lijun Ouyang, Bin Yang, Hong Zhou, and Yaping Wan. 2023. MRSCFusion: Joint Residual Swin Transformer and Multiscale CNN for Unsupervised Multimodal Medical Image Fusion. *IEEE Transactions on Instrumentation and Measurement* (2023).
- [30] Han Xu, Jiayi Ma, Junjun Jiang, Xiaojie Guo, and Haibin Ling. 2020. U2Fusion: A unified unsupervised image fusion network. *IEEE Transactions on Pattern Analysis and Machine Intelligence* 44, 1 (2020), 502–518.
- [31] Han Xu, Jiayi Ma, Zhuliang Le, Junjun Jiang, and Xiaojie Guo. 2020. FusionDn: A unified densely connected network for image fusion. In *Proceedings of the AAAI conference on artificial intelligence*, Vol. 34. 12484–12491.
- [32] Qilang Ye, Zitong Yu, Rui Shao, Xinyu Xie, Philip Torr, and Xiaochun Cao. 2024. CAT: Enhancing Multimodal Large Language Model to Answer Questions in Dynamic Audio-Visual Scenarios. *arXiv preprint arXiv:2403.04640* (2024).
- [33] Zitong Yu, Rizhao Cai, Yawen Cui, Xin Liu, Yongjian Hu, and Alex Kot. 2023. Rethinking vision transformer and masked autoencoder in multimodal face anti-spoofing. *arXiv preprint arXiv:2302.05744* (2023).
- [34] Zitong Yu, Benjia Zhou, Jun Wan, Pichao Wang, Haoyu Chen, Xin Liu, Stan Z Li, and Guoying Zhao. 2021. Searching multi-rate and multimodal temporal enhanced networks for gesture recognition. *IEEE Transactions on Image Processing* 30 (2021), 5626–5640.
- [35] Hao Zhang and Jiayi Ma. 2021. SDNet: A versatile squeeze-and-decomposition network for real-time image fusion. *International Journal of Computer Vision* 129, 10 (2021), 2761–2785.
- [36] Xingchen Zhang and Yiannis Demiris. 2023. Visible and infrared image fusion using deep learning. *IEEE Transactions on Pattern Analysis and Machine Intelligence* (2023).
- [37] Yu Zhang, Yu Liu, Peng Sun, Han Yan, Xiaolin Zhao, and Li Zhang. 2020. IFCNN: A general image fusion framework based on convolutional

- neural network. *Information Fusion* 54 (2020), 99–118.
- [38] Zixiang Zhao, Haowen Bai, Jianshe Zhang, Yulun Zhang, Shuang Xu, Zudi Lin, Radu Timofte, and Luc Van Gool. 2023. Cddfuse: Correlation-driven dual-branch feature decomposition for multi-modality image fusion. In *Proceedings of the IEEE/CVF conference on computer vision and pattern recognition*. 5906–5916.
- [39] Tao Zhou, QianRu Cheng, HuiLing Lu, Qi Li, XiangXiang Zhang, and Shi Qiu. 2023. Deep learning methods for medical image fusion: A review. *Computers in Biology and Medicine* (2023), 106959.